NJC

ROYAL SOCIETY OF CHEMISTRY

PAPER

View Article Online
View Journal | View Issue

Cite this: *New J. Chem.*, 2023, **47**, 20048

Structure elucidation of 4-carboxy-3-deoxyanthocyanidins formed from thermal degradation of hydroxyphenyl-pyranoanthocyanins†

Danielle M. Voss,[a] Fenfen Tang,[a] Kenneth M. Riedl,[abc] Gonzalo Miyagusuku-Cruzado,[a] Siyu Yao,[a] Luis Rodriguez-Saona,[a] Emmanuel Hatzakis[a] and M. Monica Giusti*[a]

Hydroxyphenyl-pyranoanthocyanins are vibrantly colored, anthocyanin-derived polyphenols found in some wines and aged juices. Upon heating (90 °C), solutions of 10-catechyl-pyranoanthocyanins (a type of hydroxyphenyl-pyranoanthocyanins) formed a unique, color producing degradation compound. This compound was produced in the greatest quantities at pH 1 and pH 3 where its formation contributed to retention of color intensity despite extensive heating conditions (up to 34 hours). We elucidated the structure of this colored compound and investigated if other hydroxyphenyl-pyranoanthocyanins produced similar colored thermal degradation products. Analysis of the isolated 10-catechyl-pyranoanthocyanin degradation compound by uHPLC-PDA, high resolution MS/MS (QTOF), FTIR, 1D and 2D NMR (^{1}H, COSY, HMBC, HSQC), spectrophotometry, and color analysis revealed that it was a 4-carboxy-3-deoxyanthocyanidin with a catechol substitution, named 4-carboxy-3-deoxycyanidin. It produced an exact mass of 315.0502 consistent with a chemical formula of $C_{16}H_{11}O_7^+$. NMR allowed for structural assignments, and key FTIR discriminating bands supported the presence of aromatic rings and the carboxylic acid moiety. The color of 4-carboxy-3-deoxycyanidin transitioned from yellow ($\lambda_{vis\text{-}max}$ = 479 nm) at pH 1 to magenta ($\lambda_{vis\text{-}max}$ = 545 nm) at pH 9.2, analogous with a flavylium system. Similarly, unique, colored degradation compounds formed from three other hydroxyphenyl-pyranoanthocyanins (10-*p*-hydroxyphenyl-, 10-guaiacyl-, and 10-syringyl-pyranoanthocyanins) each with a *m*/*z* 398 units lower than their parent pyranoanthocyanin. These findings revealed the formation of a unique class of pyranoanthocyanin derived flavylium compounds: 4-carboxy-3-deoxyanthocyanidins.

Received 15th May 2023,
Accepted 6th October 2023

DOI: 10.1039/d3nj02233a

rsc.li/njc

1. Introduction

Pyranoanthocyanins (PACNs) are a class of polyphenolic pigments found in aged red wine where they contribute to the characteristic tawny color.[1–3] They have also been found in products such as aged juices[4,5] and strawberries[6] albeit in minor amounts. The chemical structure of a PACN is comprised of an anthocyanin backbone with a second pyran ring attached at the C4 and C5–OH group (Fig. 1). This ring can form through a multistep cycloaddition reaction between an anthocyanin and a reactive cofactor such as an enolizable compound or one with a vinyl group.[2,7,8] Of the cofactors used

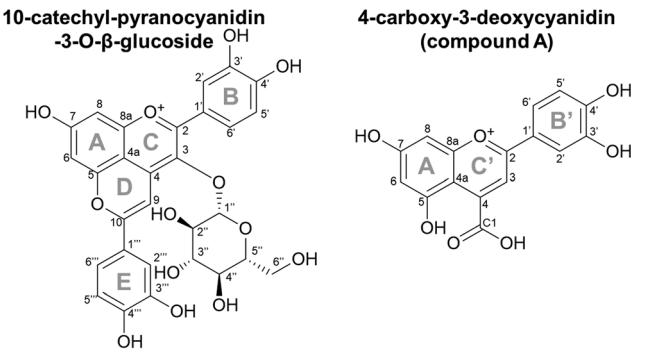

Fig. 1 Chemical structures for 10-catechyl-pyranocyanidin-3-O-β-glucoside and 4-carboxy-3-deoxycyanidin (compound **A**). Ring B′ and C′ on compound **A** were derived from the E and D rings, respectively, of 10-catechyl-pyranocyanidin-3-O-β-glucoside.

[a] *The Ohio State University, Department of Food Science and Technology, 2015 Fyffe Rd., Columbus, OH 43210, USA. E-mail: giusti.6@osu.edu; Fax: +1 614-292-0218; Tel: +1 614-247-8016*
[b] *The Ohio State University Comprehensive Cancer Center, 2015 Fyffe Rd., Columbus, OH 43210, USA*
[c] *BeaconPoint Labs, 150 N Research Campus Dr, Kannapolis, NC 28081, USA*

† Electronic supplementary information (ESI) available. See DOI: https://doi.org/10.1039/d3nj02233a

for PACN formation, hydroxycinnamic acids and their decarboxylated 4-vinylphenol counterparts form PACNs most efficiently under accelerated conditions, producing appreciable yields of hydroxyphenyl-PACNs within several days.[9,10] As efficient production methods continue to be developed, interest is growing in using hydroxyphenyl-PACNs as colorants in food and consumer packaged goods due to their vibrant color which is stable to heat,[11,12] pH changes,[13] and bleaching[14] and their antioxidant capacity.[13,15]

Recently, we reported unusual behavior of 10-catechyl-PACNs, a type of hydroxyphenyl-PACN, during thermal treatment. With heat, a unique degradation compound that absorbed light in the visible range ($\lambda_{vis\text{-}max}$ = 478 nm) formed.[11,12] Its formation likely contributed to the remarkable color stability to heat for 10-catechyl-PACNs, behavior contrasted with the rapid color loss with heat for the precursor anthocyanins and the formation of only colorless degradation compounds from 10-carboxy- and 10-methyl-PACNs.[11,12] This unique colored degradation compound formed from 10-catechyl-PACNs irrespective of the core anthocyanin type (*i.e.* cyanidin *vs.* malvidin) and was thought to contain parts of the A, D, and E ring of the parent PACN,[11,12] leading us to hypothesize that other hydroxyphenyl-PACNs could produce similar colored compounds.

Therefore, the objective of this experiment was to elucidate the chemical structure and evaluate the formation, color, and stability characteristics of the colored 10-catechyl-PACN degradation compound, referred to as compound **A** hereafter. In addition, we determined if the same type of compound is formed from three other hydroxyphenyl-PACNs. As hydroxyphenyl-PACNs have been found in products such as juice and wine[4,5,16] and with consideration for their use as colorants for consumer goods, it is necessary to further identify the degradation compound(s) as they could potentially form in PACN-containing products.

2. Experimental section

2.1. Materials

Elderberry (*Sambucus nigra*) anthocyanin color powder from DDW The Color House (Louisville, KY, USA) was used as the source of anthocyanins (primarily comprised of cyanidin-3-glucoside and cyanidin-3-sambubioside).[17] Caffeic acid, ferulic acid, and sinapic acid were obtained from TCI Chemicals (Portland, OR, USA). *p*-Coumaric acid was obtained from MP Biomedicals (Solon, OH, USA). Luteolinidin chloride standard was obtained from Extrasynthese (Genay, France). Deuterated MeOH was obtained from Acros Organics (Fair Lawn, NJ, USA).

2.2. Hydroxyphenyl-pyranoanthocyanin formation, isolation, and thermal degradation compound detection

Hydroxyphenyl-PACNs were formed following the procedure in Miyagusuku-Cruzado *et al.* with slight modifications.[9] Briefly, elderberry anthocyanins (~500 μM final concentration) were mixed with *p*-coumaric acid, caffeic acid, ferulic acid, or sinapic acid at a 1 : 30 M ratio in water adjusted to a pH of 3.1 with HCl with 0.1% potassium sorbate and 0.1% sodium benzoate preservatives. The solutions were incubated (45 °C, ~30 days) to form 10-*p*-hydroxyphenyl-, 10-catechyl-, 10-guaiacyl-, and 10-syringyl-PACNs, respectively. Incubation ended when there were little to no anthocyanins remaining. Chemical yields for PACN formation were calculated based on the PDA peak area for the PACNs at the end of the incubation period divided by the initial peak are for the ACNs as described in Miyagusuku-Cruzado *et al.*[9] The formed hydroxyphenyl-PACNs were semi-purified with solid phase extraction on C18 cartridges[18] and isolated using semi-preparatory HPLC. A Shimadzu Prominence semi-preparatory HPLC comprised of two LC-6AD pumps, CBM-20A controller, SIL-20A autosampler, and SPD-M20A PDA detector was used (Columbia, MD, USA). Separation conditions included a 12 mL min^{-1} flow rate under gradient conditions of A: 4.5% formic acid in H_2O and B: acetonitrile and a Synergi Max-RP 80 Å (250 mm × 21.2 mm i.d., 4 μm) or Luna PFP 100 Å (250 mm × 21.2 mm i.d., 5 μm) column (both from Phenomenex, Torrence, CA, USA). From the collected and diluted eluate, HPLC solvents were removed with solid phase extraction.

For degradation compound analysis, isolates of either 10-*p*-hydroxyphenyl-pyranocyanidin-3-sambubioside, 10-catechyl-pyranocyanidin-3-sambubioside, 10-guaiacyl-pyranocyanidin-3-sambubioside, or 10-syringyl-pyranocyanidin-3-sambubioside were mixed in water with a small concentration of MeOH to aid in solubility, and the pH was adjusted to 3.0 ± 0.8 and absorbance of ~1 at $\lambda_{vis\text{-}max}$. The samples were heated in a 90 °C water bath for 15 hours as performed in Voss *et al.* with each sample heated in duplicate.[11] Pigment identities and their degradation compound were identified using a Nexera-I LC2040 ultra high performance liquid chromatography system with photodiode array detection run tandem to a LCMS 8040 triple quadrupole mass spectrometer with electrospray ionization (uHPLC-PDA-ESI-MS/MS; Shimadzu, Columbia, MD, USA). Chromatographic separation was achieved with a Restek Pinnacle DB IBD column (50 mm × 2.1 mm i.d., 1.9 μm; Bellefonte, PA, USA), 50 °C column oven, and a binary gradient of solvent A: 4.5% formic acid in H_2O and solvent B: acetonitrile at a 0.25 mL min^{-1} flow at the following percentages: 0–20% B from 0 to 12 min, 20–35% B from 12 to 15 min, and 35–45% B from 15 to 16 minutes followed by column equilibration. MS/MS was conducted in positive ion mode with 2 L min^{-1} nebulizing gas, 11 L min^{-1} drying gas, 230 °C desolvation line, and 200 °C heat block. Key MS/MS programs included selective ion monitoring, product ion scans (35 eV collision energy), and a neutral loss scan for *m*/*z* of 294 (35 eV collision energy) for the sambubioside moiety. Data was processed using LabSolutions (v.5.80; Shimadzu, Columbia, MD, USA).

2.3. Compound A formation across pH values

Isolated 10-catechyl-pyranocyanidin-3-sambubioside (Section 2.2) was heated for up to 34 hours at four pH values to monitor the kinetic rate of PACN degradation and compound **A** formation. A stock solution of 10-catechyl-pyranocyanidin-3-sambubioside was prepared with 50% MeOH and 50% H_2O and aliquoted at a dilution factor 15.04 into buffers: pH 1 (0.025 M KCl adjusted

with HCl), pH 3.0 (citric acid–Na_2HPO_4), pH 5.0 (citric acid–Na_2HPO_4), and pH 7.0 (citric acid–Na_2HPO_4) all within ± 0.1 pH unit. The PACN-buffer solutions were distributed into brown microcentrifuge tubes, flushed with N_2, and placed in a water bath set to 90 °C. At each heating time point, a microcentrifuge tube was removed from heat, chilled in ice water for 2 minutes, and then let sit at room temperature for 2 minutes prior to measurements. Heating was stopped after degradation (or formation) rates plateaued or after 34 hours (pH 3).

After removing from heat, the samples were spiked with HCl to decrease the pH below 1 prior to HPLC-PDA analysis. Acidification favored the flavylium cation for both PACN and compound **A** thus removing the effect of pH on quantification. HPLC-PDA analysis was performed with a Shimadzu Prominence HPLC with two LC-20AD pumps, CBM-20A controller, SPD-M20A PDA detector, SIL-20AC autosampler, and CTO-20A column oven (Columbia, MD, USA). Separation was achieved with a Kinetex EVO C18 column (150 mm × 4.6 mm i.d., 5 μm; Phenomenex, Torrance, CA, USA) and a binary gradient of solvent A: 4.5% formic acid H_2O and solvent B: 4.5% formic acid acetonitrile at a 1.0 mL min^{-1} flow rate. The following gradient was used: 0–37% B from 0 to 10 min followed by 9 minutes of column equilibration. The peak areas of the PACNs (starting 10-catechyl-pyranocyanidin-3-sambubioside and formed 10-catechyl-pyranocyanidin-3-glucoside) and compound **A** were integrated using the 450–550 nm max plot. Each sample was injected in duplicate, and the mean values were used for calculations and analyses. Linear regression analysis of PACN degradation and compound **A** formation was performed using GraphPad Prism (v.10.0.2). A first order-kinetic fit was used to model PACN degradation. Either a first (pH 1) or zero (pH 3) order model was used for compound **A** formation with the best model selected based on a sum of squares *F*-test. Yields of compound **A** were calculated using the following formula:

$$\text{Compound A yield}\% = \frac{\text{Compound A Peak Area } T_{x(450-550\,\text{nm Max Plot})}}{\text{PACN Peak Area } T_{0(450-550\,\text{nm Max Plot})}} \times 100$$

Absorbance spectra of the heated solutions (not spiked with HCl) were measured in a 96-well UV transparent plate with a Spectra Max M2 spectrophotometer from 260 to 700 nm (5 nm step) and from 450 to 520 nm (1 nm step) with each time point plated in duplicate (Molecular Devices, San Jose, CA, USA). Spectral data was converted to CIELAB L^* (lightness), C^*_{ab} (chroma), h_{ab} (hue angle) color coordinates under D65 illuminant and 10° observer angle using ColorBySpectra software.[19] Thermal heating was performed with 3 experimental replicates but pH 3, 34 hour and pH 5, 2 hour measurements had only 2 replicates.

2.4. Formation and isolation of compound A for structure elucidation

Large amounts of compound **A** were needed for structure elucidation. For this purpose, formed 10-catechyl-PACNs (from Section 2.2) were semi-purified to remove remaining ACNs, cofactors, and preservatives (potassium sorbate and sodium benzoate) present from the PACN formation process using cation exchange chromatography[20] and solid phase extraction on C18 cartridges.[18] This semi-purified solution of 10-catechyl-PACNs was adjusted to a pH of 3.0 ± 0.05 with HCl and heated for up to 22 hours in a water bath set to 90 °C. The heated PACNs were filtered to remove the formed precipitate and semi-purified again with solid phase extraction, and formed compound **A** was isolated with semi preparatory HPLC as previously described. The semi-preparatory HPLC eluate containing compound **A** was processed and dried. For high resolution MS, nuclear magnetic resonance (NMR), and spectrophotometric and color analyses, the HPLC eluate containing compound **A** was processed using solid phase extraction and then dried with a Vacufuge Plus vacufuge (Eppendorf, Enfield, CT, USA). For Fourier transform infrared (FTIR) analysis, the eluate was dried directly using N_2 evaporation.

2.5. Structure elucidation and characterization of compound A

A multipronged approach was employed to determine the chemical structure and the color characteristics of compound **A** including uHPLC-PDA, high resolution mass spectrometry, 1D and 2D NMR, FTIR, spectrophotometry, and color measurement. Prior to each analysis, the identity and purity of compound **A** was confirmed with the uHPLC-PDA-ESI-MS/MS system, column, column oven temperature, flow rate, and mobile phase solvents described in Section 2.2. Peak purity was determined based on the equation below:

$$\text{Peak Purity}\% = \frac{\text{Compound A Peak Area}_{(260-700\,\text{nm Max Plot})}}{\text{Sum of all Peak Areas}_{(260-700\,\text{nm Max Plot})}} \times 100$$

2.5.1. High resolution mass spectrometry. Compound **A** was evaluated using quadrupole time of flight mass spectrometry (QTOF MS/MS) for exact mass determination. An Agilent 1290 Infinity II uHPLC with PDA detection coupled to an Agilent 6550 QTOF mass spectrometer was used (Agilent Technologies, Santa Clara, CA, USA). Chromatographic separation was achieved with a CSH C18 column (150 mm × 2.1 mm i.d., 1.8 μm; Waters, Milford, MA, USA), 40 °C column oven, and a binary gradient of solvent A: 5% formic acid in H_2O and solvent B: 5% formic acid in acetonitrile at 0.3 mL min^{-1} flow rate. The following gradient was used: 0% B for 1.5 min and 0–60% B from 1.5 to 15 min followed by column equilibration. The LC-PDA separation and detection were run in tandem with high resolution MS and MS/MS analyses. Parameters for MS included 150 °C drying gas at 18 L min^{-1}, 350 °C sheath gas at 12 L min^{-1}, nozzle voltage at 1000 V, and capillary voltage at 3500 V. Mass spectra were collected in both positive and negative ion mode from 30–1700 amu at ~20 000 resolution and 3 Hz. For MS/MS acquisition, both 6 and 3 Hz were used with 10, 20, and 40 eV collision energy. Profile mass data was acquired and centroided using MassHunter Acq software (ver.B.09) and analyzed with MassHunter Qual (ver.B.10; Agilent Technologies, Santa Clara, CA, USA). Calibration of the mass axis was performed using ESI-L solution with HP321 for

positive ion mode (Agilent Technologies, Santa Clara, CA, USA), and within-run calibration used m/z 1033 from HP921 and m/z 112 from trifluoroacetic acid. SIRIUS software (v.4) was used for determination of the chemical formula from the exact mass.[21]

2.5.2. Nuclear magnetic resonance. Compound **A** was re-solubilized with 0.001% HCl MeOH (LCMS grade) and re-dried to facilitate removal of residual water. Dried compound **A** was then mixed in CD_3OD, and the dissolved portion used for NMR analysis. For structural comparison and method validation, isolated 10-catechyl-pyranocyanidin-3-glucoside dissolved in CD_3OD was separately evaluated with NMR. NMR experiments were performed at 25 ± 0.10 °C using an 800 MHz Bruker NMR spectrometer equipped with triple resonance inverse helium-cooled cryoprobe with Z-Gradients (Billerica, MA, USA). 1D ^{1}H NMR was conducted using the pulse-acquire experiment with 64K complex data points and 64 scans. For some experiments, pre-saturation was used. The 2D double-quantum filtered correlated spectroscopy (DQF-COSY) was recorded using 16 scans, 2K data points in F1 and 256 data points in F2. The heteronuclear single quantum coherence (HSQC) and heteronuclear multiple bond correlation (HMBC) experiments were run with 2K data points in F1 and 256 data points in F2, and with 32 and 48 scans, respectively. Data was processed using TopSpin (v.3.6.4; Bruker, Billerica, MA, USA). The ^{1}H and ^{13}C chemical shifts assigned by 1D and 2D NMR were referenced to those of CD_3OD at 3.31 ppm and 49.00 ppm, respectively.[22]

2.5.3. Fourier transform infrared spectroscopy. In preparation for FTIR analysis, compound **A** was re-dissolved with 0.01% HCl in MeOH and re-dried to facilitate removal of residual water and formic acid present from the semi-preparatory HPLC eluate. One FTIR measurement was performed on compound **A** after 2 cycles of re-dissolution and drying (noted as R1) and an additional measurement was performed after 3 cycles of re-dissolution and drying (noted as R2) to evaluate potential changes in compound **A** during this process. For measurements, compound **A** was dissolved in 0.01% HCl MeOH, applied directly to the attenuated total reflectance (ATR) crystal, and dried with a vacuum. Multiple layers were applied and subsequently dried to fully cover the ATR crystal. Similarly, a standard of luteolinidin chloride dissolved in 0.01% HCl MeOH was applied and measured in the same way. FTIR measurements were conducted using an Agilent 4500 FTIR spectrometer with triple-reflection diamond ATR crystal with a 2 mm diameter surface area, 200 μm active area, 6 μm penetration depth, and ZnSe beam splitter (Santa Clara, CA, USA). The spectra resolution was 4 cm^{-1} with 128 background scans and 128 sample scans. Spectra were recorded from 4000 to 650 cm^{-1} and processed with Agilent MicroLab PC software (v.5.4.1939.0; Santa Clara, CA, USA). For analysis, normalized, mean-centered spectra were processed using principal component analysis (PCA) to observe the natural separation among the spectra. The loadings were used to see which variables contributed most to these differences. Data processing and analysis was performed in Pirouette® (v.4.5; Infometrix, Bothell, WA, USA).

2.5.4. Spectrophotometric, color, and stability analysis. Spectra and color expression of compound **A** were assessed in MeOH and five buffers—pH 1.0 (0.025 M KCl adjusted with HCl), pH 3.0 (citric acid–Na_2HPO_4), pH 5.0 (citric acid–Na_2HPO_4), pH 7.0 (citric acid–Na_2HPO_4), and pH 9.2 (Na_2CO_3–$NaHCO_3$) all measured to be within 0.06 units of the target pH. For measurements, compound **A** was dissolved in 0.01% HCl MeOH, sonicated for 10 minutes, diluted in buffers and MeOH at a dilution factor of 25, aliquoted to a 96-well plate sealed with a UV-transparent film to prevent evaporation, and let sit at room temperature for 30 minutes to allow the system to reach pseudo-equilibrium. Full spectra were recorded from 260 to 700 nm with a 1 nm step in a 96 well UV-plate with a spectrophotometer (defined in Section 2.3). The plate was stored at 25 °C for 24 hours following the initial measurement to assess color stability. The experiment was performed in triplicate experimental replicates, and within each replication, the sample was plated in triplicate. Color expression in MeOH was only performed in duplicate experimental replicates due to a limited quantity of compound **A**. Experimental replicates were standardized by adjusting the amount of acidified MeOH used for dissolution to target an initial absorbance of ~0.96 at $\lambda_{vis\text{-}max}$ in pH 1.0 buffer. Color data was calculated as described in Section 2.3. The total color change (ΔE^*_{ab}) was calculated from the L^*, a^*, and b^* coordinates, and a $\Delta E^*_{ab} > 5$ was the cutoff for an obvious color change.[23] For data analysis, the results were evaluated as means ± standard deviation of the 9 data points (3 experimental replicates × 3 technical replicates) to represent the spread of the data. A 1-way nested ANOVA with Tukey's multiple comparison test was used to evaluate the effect of pH on each color coordinate at time 0 with a p value <0.05 considered statistically significant. Absorbance stability over time was evaluated by comparing the percent change in absorbance intensity at the initial $\lambda_{vis\text{-}max}$ for each technical replicate. GraphPad Prism (v.9.5.1) was used for statistical analysis and graphing (Boston, MA, USA).

3. Results and discussion

3.1. Formation of compound A across pH

The thermal stability of 10-catechyl-pyranocyanidin-3-sambubioside and the formation rates of compound **A** were dependent on the pH of the solution. From pH 1 to 7, PACNs degraded following a first-order kinetic model. Compound **A** formed at these pH values; however, formation was only modeled at pH 1 (first order) and pH 3 (zero order) due to both increasing and decreasing concentrations through heating at pH 5 and 7 (Fig. 2). Assessment of pH 9 was not included because preliminary work did not detect the formation of compound **A** at that pH. At pH 1 and 3, heating 10-catechyl-pyranocyanidin-3-sambubioside resulted in partial acid hydrolysis to produce 10-catechyl-pyranocyanidin-3-glucoside (revealed by uHPLC-PDA-ESI-MS/MS analysis) (Fig. S1, ESI†). Both peak areas were included in the PACN degradation models. At pH 1, total PACN loss coincided with the formation of compound **A** as both compounds reached their kinetic plateau at ~12 hours (Fig. 2). In the subsequent 15 hours of

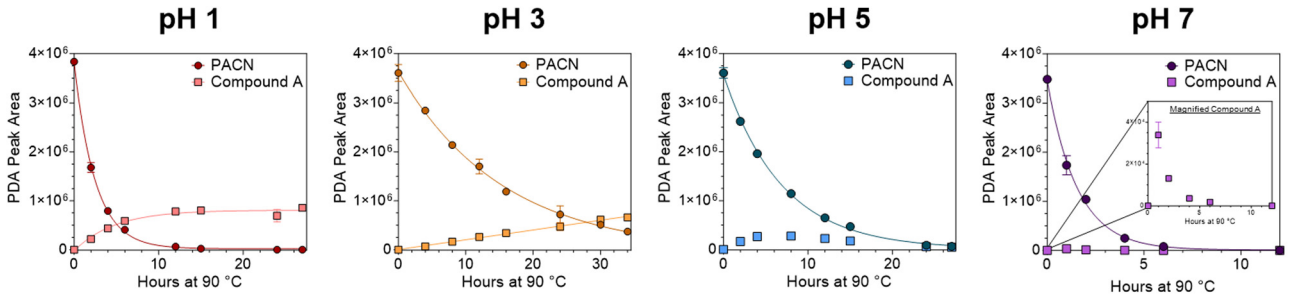

	PACN				Compound A	
	pH 1	pH 3	pH 5	pH 7	pH 1	pH 3
Kinetic Model	First	First	First	First	First	Zero
R^2	0.999	0.992	0.998	0.995	0.952	0.985
Half time (h)	1.72	10.75	4.77	1.07	3.31	No Plateau Reached
Rate (K)	0.40	0.06	0.15	0.65	0.21	19,945

Fig. 2 Changes in PDA peak area (from 450–550 nm max plot) for pyranoanthocyanins (PACN) including starting 10-catechyl-pyranocyanidin-3-sambubioside and formed 10-catechyl-pyranocyanidin-3-glucoside (pH 1 & 3) and compound **A** with 90 °C heat. Data points show mean ± standard deviation. Table shows results of kinetic model for PACN degradation and compound **A** formation.

heating there were only slight changes in compound **A** levels with largest yields obtained at the final time point of 27 hours (22.3 ± 1.1%). At pH 3, 10-catechyl-pyranocyanidin-3-sambubioside showed the greatest thermal stability, with some PACNs remaining with 34 hours of 90 °C heat (Fig. 2). Concentration of compound **A** continued to increase at the final time point of 34 hours with a yield of 17.9 ± 0.7%. As no concentration plateau was reached within this period, formation was modeled with a zero-order kinetic model. At pH 5, some 10-catechyl-pyranocyanidin-3-sambubioside remained by 27 hours of heating. The levels of compound **A** did not inversely mirror that of PACN degradation, however (Fig. 2). The greatest yields of compound **A** (7.7 ± 0.2%) were measured at 8 hours with yields decreasing over the subsequent 19 hours of heating. At pH 7, 10-catechyl-pyranocyanidin-3-sambubioside showed the lowest thermal stability, decreasing to barely detectable levels by 12 hours of heating. Only a small amount of compound **A** formed (highest yield of 1.0 ± 0.2% measured at 1 hour), but it was no longer detectable at 12 hours. Protocatechuic acid was identified to form with heating at each pH value (1, 3, 5, 7) by comparison of retention time and PDA spectra with an analytical standard.

The stability of solution color during heating was influenced both by the levels of PACN and compound **A**. Before heating, all four solutions of 10-catechyl-pyranocyaindin-3-sambubioside were orange in color (h_{ab} = 44–46°) with color intensity and $\lambda_{vis\text{-}max}$ decreasing slightly with increasing pH. With 90 °C heat,

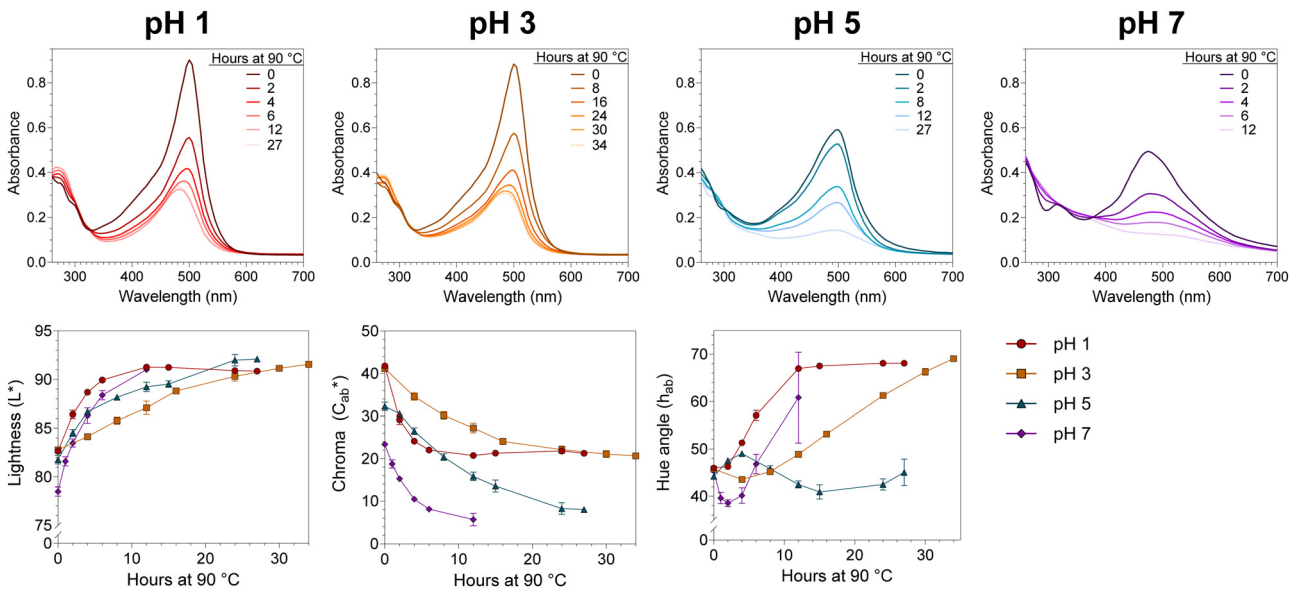

Fig. 3 Absorbance and color change of 10-catechyl-pyranocyanidin-3-sambubioside solutions in four pH buffers with 90 °C heating. Spectra show mean absorbance values taken with a 5 nm step, and L^*, C^*_{ab}, and h_{ab} data points show mean ± standard deviation.

all solutions lost orange color intensity marked by increasing L^* and decreasing C^*_{ab} and absorption at $\lambda_{vis\text{-}max}$ (Fig. 3). The pH 5 and 7 solutions were very pale at the final measured time point (27 and 12 hours, respectively) with $C^*_{ab} < 9$ (Fig. 3). At this point, these solutions had low levels of color producing compounds (PACNs and compound **A**; Fig. S1, ESI† and Fig. 2). However, for the solutions at pH 1 and pH 3, the formation of appreciable quantities of compound **A** mitigated the overall color loss. A clear hypsochromic shift in $\lambda_{vis\text{-}max}$ (501 to ~481 nm) and increase in h_{ab} by ~23° occurred (Fig. 3), coinciding with the formation trends of compound **A** in Fig. 2. For pH 1 solution, no detectable levels of PACNs remained after 12 hours, yet C^*_{ab} remained constant near 21 and the solution produced a yellow color over the subsequent 15 hours of heating, clearly demonstrating the important role of compound **A** on color retention in heated PACNs.

3.2. Identification of 10-catechyl-pyranocyanidin-3-O-β-glucoside with nuclear magnetic resonance

The identity and structure of 10-catechyl-pyranocyanidin-3-O-β-glucoside—a precursor to compound **A**—was confirmed, validating our PACN formation procedure, identification from uHPLC-PDA-MS, and NMR process. From LC-PDA-MS analysis, the $\lambda_{vis\text{-}max}$ (505 nm) and m/z (581) matched the identified 10-catechyl-pyranocyanidin-3-glucoside in Voss *et al.* which reported a $\lambda_{vis\text{-}max}$ of 505 nm and an exact mass of 581.1283.[11] The ^{1}H and ^{13}C NMR assignments of 10-catechyl-pyranocyanidin-3-glucoside were conducted using various 1D and 2D NMR experiments (Table 1). For the sugar moiety, there was a doublet at 4.78 ppm that was attributed to the anomeric proton H1″ of the sugar moiety. The ^3J coupling value of 7.7 Hz and the chemical shift indicated the presence of a β sugar. This signal had a cross peak in the COSY spectrum with a doublet of doublets at 3.68 ppm, which was assigned to hydrogen H2″ of the sugar ring.

Similarly, by combining the COSY and HMBC spectra, the signals of the remaining sugar hydrogens were assigned. The carbon chemical shifts of the sugar were assigned using the HSQC-DEPT and HMBC spectra, and the results are shown in Table 1. The ^{1}H NMR spectrum of the PACN was characterized by the presence of nine protons in the aromatic area (Fig. S2, ESI†). The singlet proton at 7.89 ppm and the anomeric proton shared an HMBC correlation peak with a quaternary carbon (C3) at 134.4. Thus, this singlet was assigned to H9 in the D ring. In addition, as shown by the COSY analysis in Fig. S3 (ESI†), the protons at 7.88 and 6.94 ppm formed an AB system, while the protons 7.70 and 6.99 ppm formed a second AB system. Additional splitting indicated the presence of protons in three AX systems. The carbon signals were assigned by the HSQC-DEPT (Fig. S4, ESI†) and HMBC (Fig. S5, ESI†). For example, the quaternary carbon C3 of the C ring appeared at 134.4 ppm while the quaternary carbon C10 of the D ring appeared at 168.6 as assigned based on its

Table 1 ^{1}H and ^{13}C NMR shifts for 10-catechyl-pyranocyanidin-3-glucoside and 4-carboxy-3-deoxycyanidin (compound **A**). Atom numbering is illustrated in Fig. 1. N/A = not applicable

10-Catechyl-pyranocyanidin-3-O-β-glucoside			4-Carboxy-3-deoxycyanidin (compound **A**)		
Atom number	δ ^{1}H ppm, J (Hz)	δ ^{13}C ppm	Atom number	δ ^{1}H ppm, J (Hz)	δ ^{13}C ppm
2	N/A	162.4			
3	N/A	134.4			
4	N/A	Not identified	4	N/A	Not identified
4a	N/A	108.0	4a	N/A	108.0
5	N/A	153.3	8a	N/A	160.0
6	7.06, d (1.3)	100.6	8	6.95, d (2.1)	96.4
7	N/A	168.4	7	N/A	171.7
8	7.10, d (1.3)	101.2	6	6.63, d (2.1)	103.9
8a	N/A	154.2	5	N/A	Not identified
9	7.89, s	97.6	3	8.00, s	108.5
10	N/A	168.6	2	N/A	172.7
1′	N/A	121.6			
2′	7.82, d (2.2)	117.5			
3′	N/A	145.9			
4′	N/A	152.2			
5′	6.94, d (8.5)	116.0			
6′	7.88, dd (8.5, 2.2)	125.0			
1″	4.78, d (7.7)	105.4			
2″	3.68, dd (7.7)	74.8			
3″	3.40, m	77.1			
4″	3.28, m	71.2			
5″	3.15, m	78.0			
6″	3.65 dd (11.4), 3.38 dd (11.4)	62.2			
1‴	N/A	122.2	1′	N/A	121.3
2‴	7.62, d (2.2)	114.7	2′	7.76, d (2.1)	115.6
3‴	N/A	147.1	3′	N/A	148.2
4‴	N/A	153.5	4′	N/A	156.7
5‴	6.99, d (8.4)	116.7	5′	7.04, d (8.6)	117.3
6‴	7.70 dd (8.4, 2.2)	122.3	6′	7.92, dd (8.6, 2.1)	125.4
			C1 (Carboxyl)	N/A	168.5

HMBC correlations with H2‴, H6‴, and H9. These ^{1}H and ^{13}C NMR shifts are similar to those reported for similar molecules such as 10-catechyl-pyranomalvidin-3-glucoside and 10-catechyl-pyranoluteolinidin with exception of the known structural differences in the B ring substitutions and C3 position, respectively.[13,24,25]

3.3. Structure elucidation of compound A

The efficient formation method of 10-catechyl-PACNs from caffeic acid cofactor developed previously[9] enabled the production of large quantities of 10-catechyl-PACNs and subsequently large quantities of compound **A** required for structure elucidation experiments. The isolated compound **A** formed for these experiments had the same LCMS characteristics ($\lambda_{vis\text{-}max}$ = 478 ± 1 nm, m/z = 315) as the compound previously reported supporting the reproducibility of formation and the retention of the compound through isolation.[11,12] Using a multifaceted approach including uHPLC-PDA, high resolution MS/MS, 1D and 2D NMR, FTIR, spectrophotometry, and color analyses, the chemical structure of the 10-catechyl-PACN degradation compound (compound **A**) was determined to correspond to 4-carboxy-2-(3,4-dihydroxyphenyl)-5,7-dihydroxychromenylium (Fig. 1). The compound is a 3-deoxyanthocyanidin with a carboxylic acid substitution at carbon 4. As the two *ortho* hydroxyl substitutions in the B′ ring are in the same position as observed for stable conformers of cyanidin,[26] compound **A** was named 4-carboxy-3-deoxycyanidin. Detailed analyses and conclusions from each characterization step are reported below.

3.3.1. High resolution mass spectrometry. The exact mass ([M^{+}]) of compound **A** was shown with high resolution MS in positive ionization to be 315.0502 m/z units, consistent with the m/z of 315 obtained with low resolution MS. This exact mass value corresponded to the chemical formula of $C_{16}H_{11}O_7^{+}$ (calculated exact mass is 315.0499). Key MS/MS fragments included the formation of 297.0393 which may correspond to the loss of a hydroxyl substitution, and a fragment at 269.0441 which may correspond to the loss of a carboxylic acid moiety (Fig. S6, ESI†). Negative ionization showed a nominal mass of 313 and a key fragment at 269 (data not shown); this fragment may correspond to the loss of COO group, further supporting the presence of a carboxylic acid moiety.

3.3.2. Nuclear magnetic resonance assignment. The purity of the compound **A** sample used for NMR was 98.95% based on uHPLC-PDA max plot peak area. NMR assignment of compound **A** was used to determine the structure and chemical connectivity, and the spectra were compared to those of 10-catechyl-pyranocyanidin-3-O-β-glucoside in Section 3.2. For comparison, both the atom numbers of stand-alone compound **A** and the original atom number for the carbon or hydrogen when it was attached to the parent molecule (10-catechyl-pyraoncyanidin-3-glucoside) are referenced below; atom numbers are found on Fig. 1. A major difference in the ^{1}H NMR spectrum of compound **A** (Fig. S7, ESI†) compared to the parent molecule was the appearance of only six protons in the aromatic region and the drifting of chemical shifts such as of H6′ which had a shift of 7.88 ppm (^{3}J = 8.5 Hz, ^{4}J = 2.2 Hz) in 10-catechyl-pyranocyaindin-3-glucoside and a shift of 7.92 ppm (^{3}J = 8.6 Hz, ^{4}J = 2.1 Hz) in compound **A**. Another difference was the absence of signals from sugar ring protons suggesting that compound **A** is not glycosylated, confirming the MS/MS results we reported previously.[11] Inspection of signal splitting in the ^{1}H NMR and COSY suggested the presence of one AB system between hydrogens at 7.92/7.04 ppm and two AX systems between hydrogens at 7.92/7.76 ppm and hydrogens at 6.95/6.63 ppm, as shown in Fig. S7 and S8 (ESI†). Further, there is an additional HMBC correlation peak for H3 (originating from H9 in the parent PACN) with a carboxylic carbon (C1) at 168.5 ppm. The most important HMBC connectivities are shown in Fig. S9 (ESI†), while the complete ^{1}H and ^{13}C chemical shift assignments are shown in Table 1. The ^{13}C chemical shifts were based on the 2D HSQC-DEPT and HMBC spectra. 1D ^{13}C NMR was also recorded, however a spectrum with high sensitivity was not obtained in a reasonable time due to low concentration. It was not possible to assign carbons C5 (originating from C8a in the parent PACN) and C4 (originating from C4 in the parent PACN) because no correlation peak was observed in the HMBC spectrum. This lack of correlation peak is potentially due to the small ^{1}H–^{13}C J coupling values or the short T_2 relaxation time of those quaternary carbons.

The NMR spectra showed several shifts consistent with acyl chains. The main impurity signals are a triplet (0.896 ppm) that is typical for a methyl group of acyl chains and a broad signal at 1.29 ppm belonging to the methylene hydrogens of the chains. These signals have correlations in COSY further confirming that they belong to the same chains. These are believed to be contaminants from the alkyl C18 chains in the separatory cartridges used to concentrate compound **A** after semi-preparatory HPLC isolation. This was supported with FTIR analysis of the cartridge methanolic eluent, showing two small bands at ∼2922 and 2852 cm^{-1} consistent with CH stretching for CH_3 and CH_2 groups (data not shown).[27–29] As they do not absorb UV or visible light, they did not appear on the 260–700 nm max plot from uHPLC-PDA analysis used to determine purity.

3.3.3. Fourier transform infrared spectroscopy. The purity of compound **A** sample used for FTIR analysis was 100% based on uHPLC-PDA 260–700 nm max plot peak area. The FTIR spectra of compound **A** and luteolinidin standard were similar, as expected based on their structural similarities with exception of the C4 carboxylic acid moiety (Fig. 4). PCA analysis helped identify the key differentiating bands where the samples naturally differed. PCA factor 1 described differences between compound **A** replicates and luteolinidin standard, with the main differences associated with bands at 1548, 1525, 1402, 1324, 1275, and 1151 cm^{-1} (Fig. 4). The bands at 1548 and 1525 cm^{-1} fall within the region associated with C=C stretching of aromatic rings.[27,30] The band at 1402 cm^{-1} may relate to symmetrical stretching of the COO^{-} group as previous work has correlated these vibrations to bands ∼1380–1390 cm^{-1}.[31–33] While compound **A** was dried with acidic MeOH, it is possible for the carboxylic acid moiety to be present both in its protonated (COOH) and deprotonated (COO^{-}) form as compound **A** is believed to have a low pK_a (discussed in Section 3.3.4). Both the 1324 and 1275 cm^{-1} bands may relate to

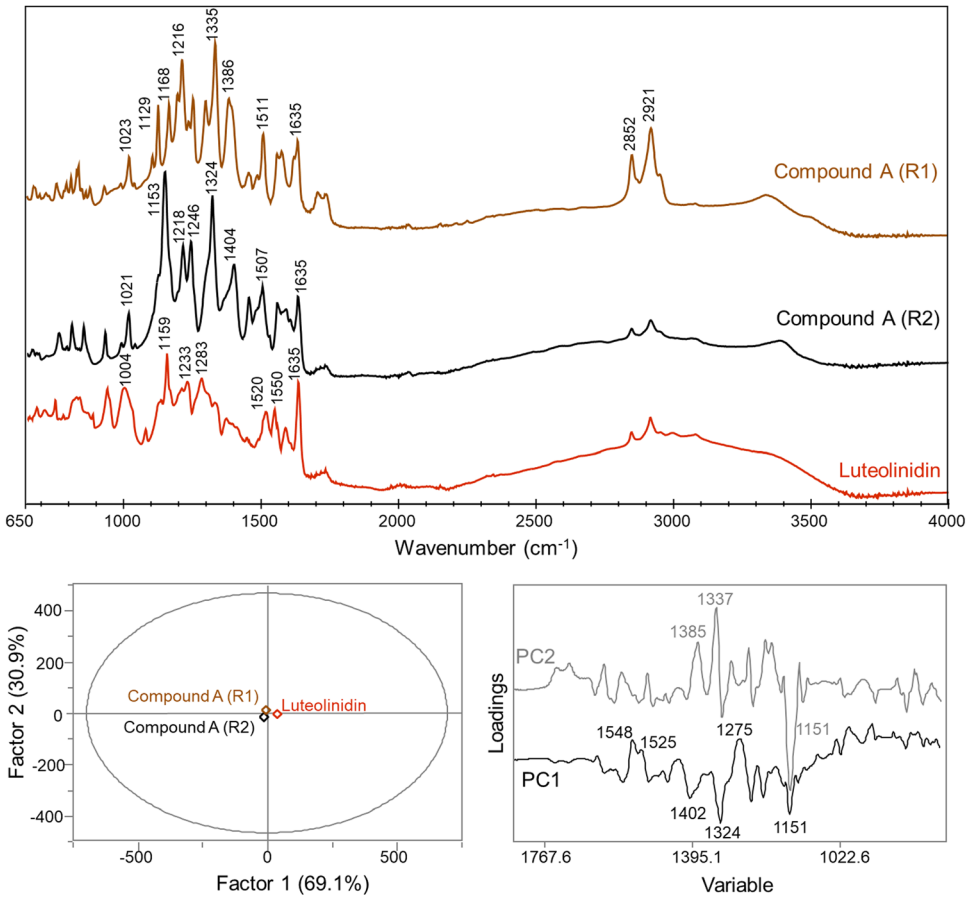

Fig. 4 FTIR spectra for 4-carboxy-3-deoxycyanidin (compound **A**) repetition 1 (R1) and 2 (R2) and luteolinidin standard and the calculated PCA plot and differentiating loadings between the three samples.

the C(phenolic)–O(H) vibrations.[30–32,34] The band at 1151 cm^{-1} may relate to COC stretching on the C ring of compound **A**.[30,34–36] The slight differences in our reported wavenumbers compared to previous FTIR analysis of phenolic compounds may be due to the unique structure of compound **A**. These observations of the FTIR spectrum suggested that the differentiating structural attributes between compound **A** and luteolinidin are related to substitutions on the aromatic ring, specifically the C′ ring, and supported the presence of a carboxylic acid moiety.

PCA factor 2 accounted for differences between the two replicates of compound **A** with key differentiation bands at 1385, 1337, and 1151 cm^{-1} (Fig. 4). Differences between the two replicates may be due to changes in non-covalent interactions that could be altered and disrupted during the re-solution and drying process. The bands at 1385 and 1337 cm^{-1} may be related either to the COO^{-} group or C(phenolic)–O(H) group, as previously discussed, with both functional groups highly prone to intermolecular interactions. Previous work with phenolic compounds has shown that shifts within this range may be due to complexation with metal ions.[31,36,37] Trace metals may have been present in the sample and changes in the complexation of compound **A** with these ions may have occurred with the subsequent re-dissolution and drying cycle. These differences between the two measurements for compound **A** support the structural assignment as 4-carboxy-3-deoxycyanidin.

3.3.4. UV-visible absorbance and color expression across pH. uHPLC-PDA analysis of compound **A** both in this and our previous work[11,12] showed strong absorbance in the visible range ($\lambda_{vis\text{-}max}$ of 478–479 nm) consistent with a yellow color. These observations led us to further investigate the color expressed by isolated compound **A** across pH values. The solution of compound **A** used for color analysis was ~95.7% pure based on the 260–700 nm max plot from uHPLC-PDA analysis. At acidic pH values, compound **A** appeared yellow with the $\lambda_{vis\text{-}max}$ reported by spectrophotometry similar to the values observed by uHPLC-PDA analysis in the acidic mobile phase. As the pH increased, there was a bathochromic shift in $\lambda_{vis\text{-}max}$ and a decrease in hue angle as the color transitioned to orange at pH 5 and then to magenta by pH 9.2 (Fig. 5). At pH 5 and 7, small shoulders were observed at ~410–430 and ~410–440 nm, respectively. A strong shoulder from ~470–490 nm was observed in the spectrum at pH 9.2.

The different colors produced by compound **A** across pH values is consistent with the pH-dependent structure chemistry of flavylium systems As the pH of the environment increases, the flavylium cation can be deprotonated to form a quinoidal base, and the flavylium cation can by hydrated followed by tautomerization to form the hemiketal and chalcone, with the

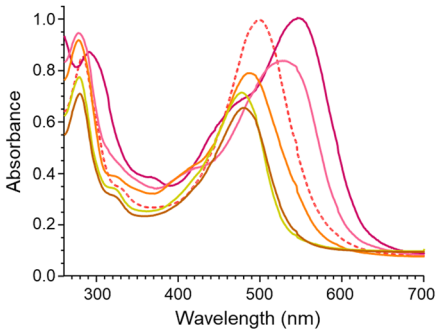

Solution	Graph Legend	$\lambda_{vis\text{-}max}$ (nm)	L*	C_{ab}*	h_{ab}
pH 1		479	83.1 ± 0.8[a]	36.3 ± 5.5[a]	70.8 ± 0.8[a]
pH 3		477	83.6 ± 1.7[a]	40.3 ± 11.4[a]	77.9 ± 0.6[b]
pH 5		486	76.5 ± 1.0[b]	41.2 ± 2.4[a]	49.0 ± 0.5[c]
pH 7		527	62.5 ± 1.6[c]	45.3 ± 1.6[a]	0.2 ± 0.5[d]
pH 9.2		545	54.0 ± 4.0[d]	44.3 ± 3.0[a]	351.7 ± 0.8[e]
MeOH		499	70.3 ± 0.5	44.5 ± 0.4	27.2 ± 0.5

Fig. 5 Spectral and CIELAB L^*, C^*_{ab}, h_{ab} values of 4-carboxy-3-deoxycyanidin (compound **A**) in pH buffers 1–9.2 and MeOH. Spectra shows mean absorption values and color characteristics are expressed as mean ± standard deviation. Different letters show statistical difference ($p < 0.05$) within a column (MeOH not included).

extent of occurrence for each of these reactions dependent on the type and number of substitutions.[38,39]

Previous work by other authors with the synthetic 4-carboxy-7-hydroxy-4′-methoxy flavylium chloride (CHMF) compound showed that at low pH values, the carboxylic carbon could be deprotonated (pK_a 0.73) to form a zwitterion, with this change causing a hypsochromic shift in $\lambda_{vis\text{-}max}$.[40] As pH increased for CHMF zwitterion, the anionic quinoidal base formed (∼pK_a 4.8), accompanied by a bathochromic shift in $\lambda_{vis\text{-}max}$.[40] These color changes match those observed for compound **A** from pH 1–7 and suggest similar structural changes occurred with pH adjustments. The color of compound **A** continued to shift to a more magenta hue with increasing pH, noted by decreasing h_{ab} and increasing $\lambda_{vis\text{-}max}$. These color changes may be due to continued deprotonation of hydroxyl substitutions to form the dianionic quinoidal base structure and re-equilibration of the multistate chemical structures.[39,41]

There was surprisingly no color fading in the mildly acidic pH range (pH 3–7) for compound **A**. Instead, as pH increased, the color became darker, supported by significant decreases in L^* ($p < 0.05$) (except between pH 1 and 3 ($p = 0.99$)) and increases in absorbance intensity at the $\lambda_{vis\text{-}max}$. There was no significant change in C^*_{ab} with increasing pH ($p = 0.43$), indicating that the color vibrancy remained the same among pH values. For flavylium compounds, lack of a substitution at C3 position and/or presence of a substitution at C4 are structural attributes both shown to improve color retention across pH values.[41–43] These substitutions are not expected to eliminate color loss as related compounds do show some hydration-initiated color fading in the mildly acidic pH range.[41,43,44] However, this reaction may be masked in our findings as the initial spectral measurement for compound **A** was recorded after 30 minutes of equilibration time, and the color was visually observed to fade during this period for pH 1 and 3. Nevertheless, as pH increased, deprotonation was likely the dominant reaction occurring rather than hydration. This supports conclusions by previous authors working with related 4-substituted flavyliums.[41,43,44] The current spectral observations and the analogous behavior to related compounds provided additional support for identification of compound **A** as 4-carboxy-3-deoxycyanidin.

3.4. Isolated compound A color stability at 25 °C

While color intensity for isolated compound **A** was retained across pH values, the color noticeably faded in 24 hours by at least 44% in all pH solutions tested except for pH 7 (Fig. 6). At pH 7, the color was remarkably stable at room temperature, with a loss of absorption at $\lambda_{vis\text{-}max}$ of just ∼7%. This exceptional pH 7 stability is consistent with the findings in Sweeny and Iacobucci for a synthetic 4-carboxy-3-deoxyanthocyanidin, which differed in structure from compound **A** only by substitutions in the B′ ring.[45] The color of compound **A** was also stable

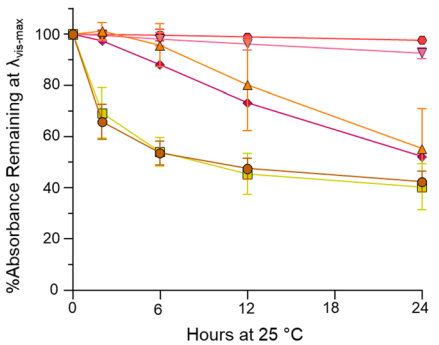

Solution	Color Parameter Change Between 0 and 24 hours			
	ΔL*	ΔC^*_{ab}	Δh_{ab}	ΔE^*_{ab}
pH 1	4.2 ± 1.0	-23.7 ± 3.6	-2.3 ± 0.6	24.1 ± 3.7
pH 3	3.6 ± 1.7	-27.8 ± 9.5	-2.7 ± 0.6	28.0 ± 9.6
pH 5	6.1 ± 2.5	-18.9 ± 7.5	-0.7 ± 0.2	19.9 ± 7.9
pH 7	1.3 ± 0.5	-3.0 ± 0.7	-0.4 ± 0.8	3.3 ± 0.9
pH 9.2	14.3 ± 0.5	-24.3 ± 1.2	6.0 ± 0.8	28.3 ± 1.2
MeOH	0.5 ± 0.1	-0.3 ± 0.3	3.0 ± 0.3	2.4 ± 0.2

Fig. 6 Color stability of 4-carboxy-3-deoxycyanidin (compound **A**) in pH from 1–9.2 buffers and MeOH over 24 hours. The graph shows the percent absorption change at $\lambda_{vis\text{-}max}$, and the table displays the change in CIELAB color coordinates with results presented as means with standard deviation.

in MeOH, in which the absorbance dropped by ~2% and there was no observable color change over 24 hours (Fig. 6).

Stability at pH 1 and 3 followed similar trends with absorbance at $\lambda_{vis\text{-}max}$ decreasing rapidly (~30–34%) in the first 2 hours. In contrast, at pH 5, most absorbance decrease happened after 6 hours. Only two experimental replicates were included for stability analysis at pH 5 as one experimental replicate showed different behavior; this replicate showed no decrease in absorbance at $\lambda_{vis\text{-}max}$ and a ΔE^*_{ab} of only 0.52. Additional research is needed to investigate the stability observed for this one experimental replicate. At all 3 acidic pH values, absorbance decreased at all wavelengths during the 24 hours (Fig. S10, ESI†), and the observable color change was driven by color fading (increasing L^* and decreasing C^*_{ab}) (Fig. 6). Different trends were observed at pH 9.2. Here, the spectral shape changed over time as absorbance increased in the ~260–280 nm and 320–400 nm ranges while decreasing at the $\lambda_{vis\text{-}max}$ (Fig. S10, ESI†). In addition to color fading (increasing L^* and decreasing C^*_{ab}), the hue increased by ~6 units over 24 hours (Fig. 6). These changes in spectral shape and hue angle may indicate that the chemical structure equilibriums are transforming over 24 hours in the high alkaline pH range.

3.5. Identification of degradation compounds from hydroxyphenyl-pyranoanthocyanins and insight into the degradation mechanism

In addition to 10-catechyl-PACNs, 10-*p*-hydroxyphenyl-, 10-guaiacyl-, and 10-syringyl-PACNs derived from cyanidin-3-sambubioside were formed with chemical yields from elderberry ACN extracts at

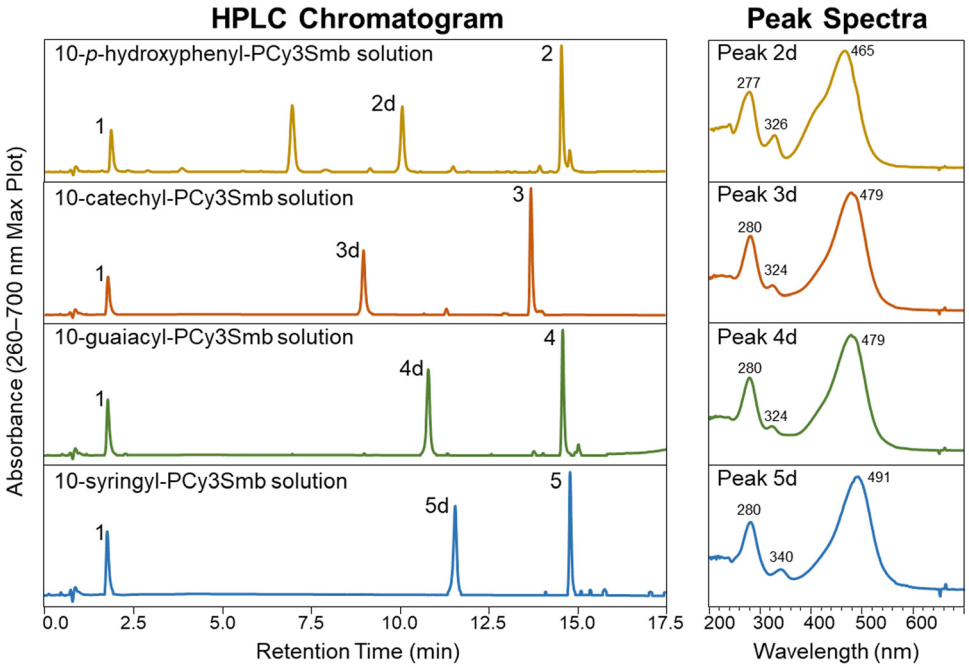

Compound/Peak #	Identity	λ_{max}	m/z
1	protocatechuic acid	259	nd
2d	4-carboxy-3-deoxypelargonidin	465	299
2	10-*p*-hydroxyphenyl-pyranoCy3Smb	500	697
3d (compound **A**)	4-carboxy-3-deoxycyanidin	479	315
3	10-catechyl-pyranoCy3Smb	506	713
4d	4-carboxy-3-deoxypeonidin	479	329
4	10-guaiacyl-pyranoCy3Smb	507	727
5d	4-carboxy-3-deoxymalvidin	491	359
5	10-syringyl-pyranoCy3Smb	512	757

nd = not detected
Cy3Smb = cyanidin-3-sambubioside

Fig. 7 uHPLC-PDA-MS characteristics of hydroxyphenyl-pyranoanthocyanins (peaks 2–5) and their thermal degradation compounds (peaks 1 and 2d–5d) following 15 hours of 90 °C heating at pH 3.0. 10-*p*-Hydroxyphenyl-pyranoCy3Smb solution contained an impurity (~6.8 min) present both before and after heating. Chromatographic conditions are provided in Section 2.2.

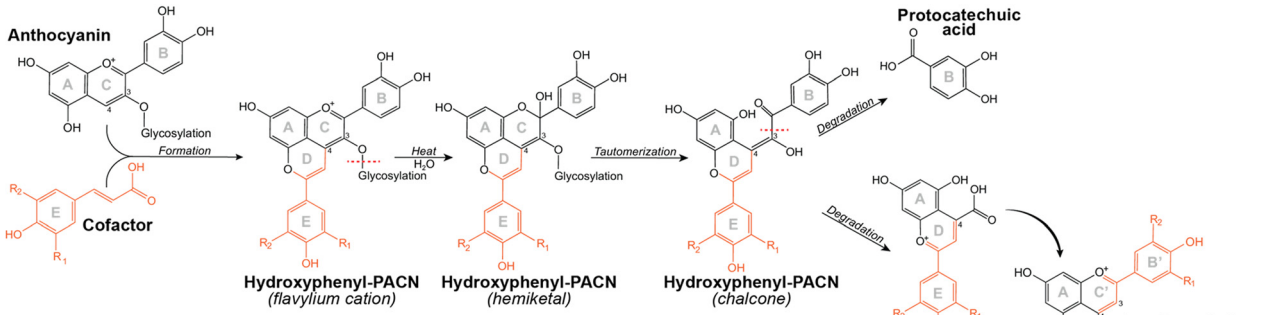

Cofactor	Formed PACN	R_1	R_2	Degradation Compound
p-coumaric acid	10-*p*-hydroxyphenyl-pyranocyanidin-3-glycoside	H	H	4-carboxy-3-deoxypelargonidin
caffeic acid	10-catechyl-pyranocyanidin-3-glycoside	OH	H	4-carboxy-3-deoxycyanidin
ferulic acid	10-guaiacyl-pyranocyanidin-3-glycoside	OCH_3	H	4-carboxy-3-deoxypeonidin
sinapic acid	10-syringyl-pyranocyanidin-3-glycoside	OCH_3	OCH_3	4-carboxy-3-deoxymalvidin

Fig. 8 Proposed schematic for hydroxyphenyl-PACN formation and thermal degradation into the 4-carboxy-3-deoxyanthocyanidin degradation compound. Rings B′ and C′ correspond to ring E and D of the parent compound, respectively.

~33.2%, 45.2%, and 39.1%, respectively. The pigments were isolated, and the reported PDA spectra, *m*/*z*, and MS/MS values of the four hydroxyphenyl-PACNs, differing only in E ring substitutions, matched the expected values and data reported for similar PACNs (Fig. 7).[46] During heating, each hydroxyphenyl-PACN formed a unique, colored degradation compound (peak 2d, 3d, 4d, 5d in Fig. 7) with the compound from 10-catechyl-pyranocyanidin-3-sambubioside (peak 3d) matching compound **A**. The differences in characteristics ($\lambda_{vis\text{-}max}$, *m*/*z*, retention time) among the four degradation compounds followed similar patterns observed for the parent PACNs. Namely, 4-carboxy-3-deoxypelargonidin (peak 2d) had the lowest $\lambda_{vis\text{-}max}$, 4-carboxy-3-deoxymalvidin (peak 5d) had the highest $\lambda_{vis\text{-}max}$, and all spectra included minor peaks near 280 nm and 324–340 nm (Fig. 7). The shape of the spectra of 4-carboxy-3-deoxypelargonidin (peak 2d) showed a slight shoulder near 415 nm, and while the wavelengths are hypsochromically shifted, the spectral shape is similar to the appearance of pelargonidin anthocyanins which often have a characteristic shoulder near 440 nm.[47] Each degradation compound had a *m*/*z* 398 units lower than their parent PACN which would support the loss of the sambubioside sugar moiety and B ring (Fig. 8). Additionally, the *m*/*z* difference among the compounds was the same as for the parent PACNs, indicating that the degradation compounds differed in structure by the E ring substitutions. Protocatechuic acid (peak 1) formed in all 4 of the heated PACNs (Fig. 7), tentatively identified based on the spectral characteristics and retention time. Protocatechuic acid is reported to form from the B ring of the heated pigment and has previously been found in solutions of heated cyanidin anthocyanins and cyanidin-derived PACNs.[12,48,49] Interestingly, our structure for peak 5d, 4-carboxy-3-deoxymalvidin, matches the theoretical compound proposed as a stable flavylium compound in Amić *et al.*;[50] these authors proposed a $\lambda_{vis\text{-}max}$ of 497.8 nm for the compound, which is slightly higher than our experimental value of 491 nm.

Elucidation of the structure of compound **A**/peak 3d provided supporting evidence for the proposed thermal degradation pathway for PACNs (Fig. 8). This pathway is postulated to involve hydration at C2 of the flavylium cation PACN to form a hemiketal, tautomerization to the chalcone, and subsequent breakage to form the B ring containing protocatechuic acid and 4-carboxy-3-deoxyanthocyanidin, based on the present findings, ACN thermal degradation pathway,[49,51] and hypotheses in Voss *et al.* and Voss *et al.*[11,12] Additionally, uHPLC-PDA-MS analysis of heated 10-catechyl-pyranomalvidin-3-glucoside/3-rutionside PACNs detected MS signals in both positive (*m*/*z* = 481.1) and negative (*m*/*z* = 479.1) mode consistent with a hydrated PACN aglycone (+18 *m*/*z* units from the aglycone) which corresponded to a small PDA peak absorbing in the 300–400 nm region (Fig. S11, ESI†). These signals were found only in the heated PACN sample with LCMS analysis using non-acidified mobile phases and supported the possibility of a chalcone or hemiketal forming during heating.

The similarities among the degradation compounds from the four hydroxyphenyl-PACNs and identification of protocatechuic acid in all four heated samples suggested that the PACNs degraded in the same manner and the structure of the colored degradation compounds are the same apart from the substitutions on the B′ ring (Fig. 8).

4. Conclusion

The colored degradation compound obtained from heat stress of 10-catechyl-PACNs was discovered to be a 4-carboxy-3-deoxycyanidin, as evidenced by uHPLC-PDA, high resolution-MS/MS, NMR, FTIR, spectrophotometry, and color results. Similar compounds were observed to form from heating other hydroxyphenyl-PACNs (10-*p*-hydroxyphenyl, 10-guaiacyl, 10-syringyl). These observations show the discovery of a unique class of 4-substituted flavylium compounds, the 4-carboxy-3-deoxyanthocyanidins, formed from nature-derived ingredients.

Data availability

The data supporting this experiment has been included in the manuscript and supplements. Additional data may be shared upon reasonable request.

Conflicts of interest

The authors declare no competing interests.

Acknowledgements

The authors would like to thank Molly J. Davis for editing this manuscript. This research was supported in part by the USDA National Institute of Food and Agriculture, Hatch Project OHO01423, Accession number 1014136 and by state and federal funds appropriated to The Ohio State University, College of Food, Agricultural, and Environmental Sciences, Ohio Experiment Station through the CFAES IGP Graduate Program (Proposal 2022-079).

References

1 P.-J. Cameira-dos-Santos, J. M. Brillouet, V. Cheynier and M. Moutounet, *J. Sci. Food Agric.*, 1996, **70**, 204–208.
2 H. Fulcrand, P.-J. Cameira-dos-Santo, P. Sarni-Manchado, V. Cheynier and J. Favre-Bonvin, *J. Chem. Soc., Perkin Trans. 1*, 1996, 735–739.
3 X.-K. Zhang, Y.-B. Lan, Y. Huang, X. Zhao and C.-Q. Duan, *Food Chem.*, 2021, **339**, 127795.
4 S. Hillebrand, M. Schwarz and P. Winterhalter, *J. Agric. Food Chem.*, 2004, **52**, 7331–7338.
5 M. Schwarz, V. Wray and P. Winterhalter, *J. Agric. Food Chem.*, 2004, **52**, 5095–5101.
6 Ø. M. Andersen, T. Fossen, K. Torskangerpoll, A. Fossen and U. Hauge, *Phytochemistry*, 2004, **65**, 405–410.
7 M. Schwarz, T. C. Wabnitz and P. Winterhalter, *J. Agric. Food Chem.*, 2003, **51**, 3682–3687.
8 V. De Freitas and N. Mateus, *Anal. Bioanal. Chem.*, 2011, **401**, 1467–1477.
9 G. Miyagusuku-Cruzado, D. M. Voss and M. M. Giusti, *Int. J. Mol. Sci.*, 2021, **22**, 6708.
10 G. Miyagusuku-Cruzado, D. M. Voss, T. N. Ortiz-Santiago, Y. Chen and M. M. Giusti, *Food Chem.*, 2023, **427**, 136705.
11 D. M. Voss, G. Miyagusuku-Cruzado and M. M. Giusti, *npj Sci. Food*, 2022, **6**, 16.
12 D. M. Voss, G. Miyagusuku-Cruzado and M. M. Giusti, *Food Chem.*, 2023, **403**, 134305.
13 J. Sun, X. Li, H. Luo, L. Ding, X. Jiang, X. Li, R. Jiao and W. Bai, *J. Agric. Food Chem.*, 2020, **68**, 2783–2794.
14 A. E. Håkansson, K. Pardon, Y. Hayasaka, M. de Sa and M. Herderich, *Tetrahedron Lett.*, 2003, **44**, 4887–4891.
15 J. Azevedo, J. Oliveira, L. Cruz, N. Teixeira, N. F. Brás, V. De Freitas and N. Mateus, *J. Agric. Food Chem.*, 2014, **62**, 7002–7009.
16 M. Á. Pozo-Bayón, M. Monagas, M. C. Polo and C. Gómez-Cordovés, *J. Agric. Food Chem.*, 2004, **52**, 1300–1306.
17 X. Wu, L. Gu, R. L. Prior and S. McKay, *J. Agric. Food Chem.*, 2004, **52**, 7846–7856.
18 L. E. Rodríguez-Saona and R. E. Wrolstad, in *Current Protocols in Food Analytical Chemistry*, ed. R. E. Wrolstad, T. E. Acree, H. An, E. A. Decker, M. H. Penner, D. S. Reid, S. J. Schwartz, C. F. Shoemaker and P. Sporns, John Wiley & Sons, Inc., Hoboken, NJ, USA, 2001, p. F1.1.1.
19 J. E. Farr and M. M. Giusti, *ColorBySpectra-Academic License, Tech License Express*, Ohio State Innovation Foundation, Columbus, OH, 2017.
20 G. Miyagusuku-Cruzado, D. M. Voss and M. M. Giusti, *Polyphenols Communications*, 2021, vol. 1, pp. 113–115. **https://www.groupepolyphenols.com/wp-content/uploads/2021/10/Polyphenols-Communications-e-vol-1-no-1.pdf**.
21 K. Dührkop, M. Fleischauer, M. Ludwig, A. A. Aksenov, A. V. Melnik, M. Meusel, P. C. Dorrestein, J. Rousu and S. Böcker, *Nat. Methods*, 2019, **16**, 299–302.
22 G. R. Fulmer, A. J. M. Miller, N. H. Sherden, H. E. Gottlieb, A. Nudelman, B. M. Stoltz, J. E. Bercaw and K. I. Goldberg, *Organometallics*, 2010, **29**, 2176–2179.
23 J. M. Obón, M. R. Castellar, M. Alacid and J. A. Fernández-López, *J. Food Eng.*, 2009, **90**, 471–479.
24 A. Vallverdú-Queralt, E. Meudec, N. Ferreira-Lima, N. Sommerer, O. Dangles, V. Cheynier and C. Le Guernevé, *Food Chem.*, 2016, **199**, 902–910.
25 L. Cruz, J. L. C. Sousa, A. Marinho, N. Mateus and V. de Freitas, *Tetrahedron Lett.*, 2017, **58**, 159–162.
26 M. Rusishvili, L. Grisanti, S. Laporte, M. Micciarelli, M. Rosa, R. J. Robbins, T. Collins, A. Magistrato and S. Baroni, *Phys. Chem. Chem. Phys.*, 2019, **21**, 8757–8766.
27 C. Shiroma-Kian, D. Tay, I. Manrique, M. M. Giusti and L. E. Rodriguez-Saona, *J. Agric. Food Chem.*, 2008, **56**, 9835–9842.
28 M. K. Trivedi, A. B. Dahryn Trivedi and H. S. Khemraj Bairwa, *Nat. Prod. Chem. Res.*, 2015, **3**, 1000186.
29 M. Lucarini, A. Durazzo, J. Kiefer, A. Santini, G. Lombardi-Boccia, E. B. Souto, A. Romani, A. Lampe, S. F. Nicoli, P. Gabrielli, N. Bevilacqua, M. Campo, M. Morassut and F. Cecchini, *Foods*, 2020, **9**, 10.
30 O. Abbas, G. Compère, Y. Larondelle, D. Pompeu, H. Rogez and V. Baeten, *Vib. Spectrosc.*, 2017, **92**, 111–118.
31 X. H. Guan, C. Shang and G. H. Chen, *Chemosphere*, 2006, **65**, 2074–2081.
32 M. V. Biber and W. Stumm, *Environ. Sci. Technol.*, 1994, **28**, 763–768.
33 M. I. Tejedor-Tejedor, E. C. Yost and M. A. Anderson, *Langmuir*, 1992, **8**, 525–533.
34 G. Tondi and A. Petutschnigg, *Ind. Crops Prod.*, 2015, **65**, 422–428.
35 S. Agatonovic-Kustrin, D. W. Morton and A. P. M. Yusof, *Mod. Chem. Appl.*, 2013, **1**, 1000110.
36 H. Dong, X. Yang, J. He, S. Cai, K. Xiao and L. Zhu, *RSC Adv.*, 2017, **7**, 53385–53395.
37 M. C. Alvarez-Ros, S. Sánchez-Cortés and J. V. García-Ramos, *Spectrochim. Acta, Part A*, 2000, **56**, 2471–2477.
38 R. Brouillard and J.-E. E. Dubois, *J. Am. Chem. Soc.*, 1977, **99**, 1359–1364.
39 L. Cruz, N. Basílio, N. Mateus, V. De Freitas and F. Pina, *Chem. Rev.*, 2022, **122**, 1416–1481.
40 L. Paulo, A. A. Freitas, P. F. Da Silva, K. Shimizu, F. H. Quina and A. L. Maçanita, *J. Phys. Chem. A*, 2006, **110**, 2089–2096.
41 J. Baranac, D. Amic and V. Vukadinovic, *Food Chem.*, 1990, **38**, 932–936.

42 J. M. Awika, L. W. Rooney and R. D. Waniska, *J. Agric. Food Chem.*, 2004, **52**, 4388–4394.
43 D. Davidović-Amić, D. Amić and N. Trinajstić, *Croat. Chem. Acta*, 1994, **67**, 163–170.
44 G. Mazza and R. Brouillard, *J. Agric. Food Chem.*, 1987, **35**, 422–426.
45 J. G. Sweeny and G. A. Iacobucci, *J. Agric. Food Chem.*, 1983, **31**, 531–533.
46 D. Blanco-Vega, F. J. López-Bellido, J. M. Alía-Robledo and I. Hermosín-Gutiérrez, *J. Agric. Food Chem.*, 2011, **59**, 9523–9531.
47 M. M. Giusti and R. E. Wrolstad, *J. Food Sci.*, 1996, **61**, 322–326.
48 E. Sadilova, R. Carle and F. C. Stintzing, *Mol. Nutr. Food Res.*, 2007, **51**, 1461–1471.
49 L. Cabrita, V. Petrov and F. Pina, *RSC Adv.*, 2014, **4**, 18939–18944.
50 D. Amić, D. Davidović-Amić, D. Bešlo, B. Lučić and N. Trinajstić, *J. Chem. Inf. Comput. Sci.*, 1999, **39**, 967–973.
51 R. Brouillard and B. Delaporte, *J. Am. Chem. Soc.*, 1977, **99**, 8461–8468.

